NMR, Crystal Structure and FAB Mass Spectral Studies of Morpholinomethylphosphonic Acid

Mark P. Lowe, Joyce C. Lockhart,* Craig J. Matthews, William Clegg, Mark R. J. Elsegood and Lynne Horsburgh
Department of Chemistry, University of Newcastle upon Tyne, Newcastle upon Tyne, UK NE1 7RU

The pD behaviour of morpholinomethylphosphonic acid has been investigated using multinuclear NMR (^1H, ^{13}C and ^{31}P) techniques in D_2O solvent. The molecule, found to exist in a zwitterionic form, consisting of a weakly deuteriated basic nitrogen and strongly acidic phosphonic acid groups, showed a dramatic change in the NMR spectra as the nitrogen was dedeuteriated. At low pD when the ring is in a state of slow exchange, complex coupling patterns for the $(ABCD)_2$ spin system are observed. However as the pD was raised broad featureless spectra were obtained and finally at higher values of pD deceptively simple coupling patterns for a new spin $(AA'BB')_2$ system were observed, corresponding to a conformationally mobile ring in fast exchange. The zwitterionic nature of the molecule was also highlighted in the X-ray crystal structure of the monohydrate which revealed hydrogen-bonded dimers, and was also observed in the FAB mass spectrum, where aggregates of molecules were noted at masses of $(M + 1)^+$, $(2M + 1)^+$, $(3M + 1)^+$ and $(4M + 1)^+$. In the crystal structure, further hydrogen bonding involving the water of crystallisation produces a three-dimensional network.

Recent work[1,2] on aminomethylenephosphonic acids ($RR'NCH_2PO_3H_2$) has indicated the importance of NMR studies in the unravelling of the complex equilibria. It was important for us, in relation to our self-assembly studies of their polyoxometallate conjugates[3] to appreciate fully the spectra of the phosphonic acids alone in order to interpret spectra of the derived conjugates. For small polyaza macrocycles with multiple phosphonic acid groups, the overlap of the pH ranges in which the pK_as of individual amino or phosphonic acid groups fall, made interpretation very difficult.[4] Lukeš recently examined the piperidinylmethylphosphinic acid with more success.[5] We present here the multinuclear NMR studies for morpholinomethylphosphonic acid (**1**) as the acidity of the

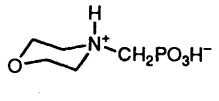

1

solution is varied and interpret the results in terms of processes occurring in solution. The nature of hydrogen bonding in the solid state emerges from the X-ray crystal structure also presented for the hydrate, and this is used in turn to interpret curious dimers and other oligomers found in the FAB mass spectrum.

Results and Discussion

NMR Studies.—For morpholinomethylphosphonic acid there are three conventional equilibria in aqueous solution. These are shown in Scheme 1 [eqns. (1)–(3)]. The pK_as of these equilibria range from the typical amine[6] pK_a values (*ca.* 12–8) to typical phosphonate[1] values (4–0). These equilibria may overlap in the pD ranges in which they occur (see Scheme 1). In addition to the three deuteriation equilibria shown, the heterocyclic ring is subject to the additional equilibria shown in eqns. (4) and (5) (Scheme 1). The six-membered ring is fluxional with interconversion of equatorial and axial positions in the chair form, the steric preference of the $CH_2PO_3^{2-}$ group being equatorial. Additionally there is inversion at the

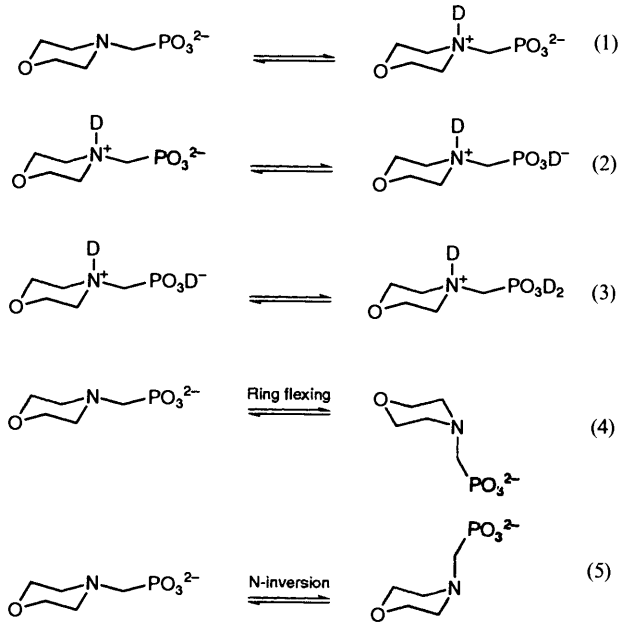

Scheme 1 Solution equilibria for aminomethylphosphonic acids

Slow Exchange Region	Intermediate Exchange Region	Fast Exchange Region
Sharp individual signals	Broad humps	Sharp signals (weighted average)

Scheme 2 Regions of exchange and their relation to NMR signals

nitrogen atom. Since there are multiple equilibria there are also multiple rate processes. The three regions of exchange are highlighted in Scheme 2. When the pD of the solution is several units below the pK_a, the proton exchange is observably slow on the NMR timescale. At very low pD, the heterocyclic ring will be effectively static, and at very high pD the ring motion will be

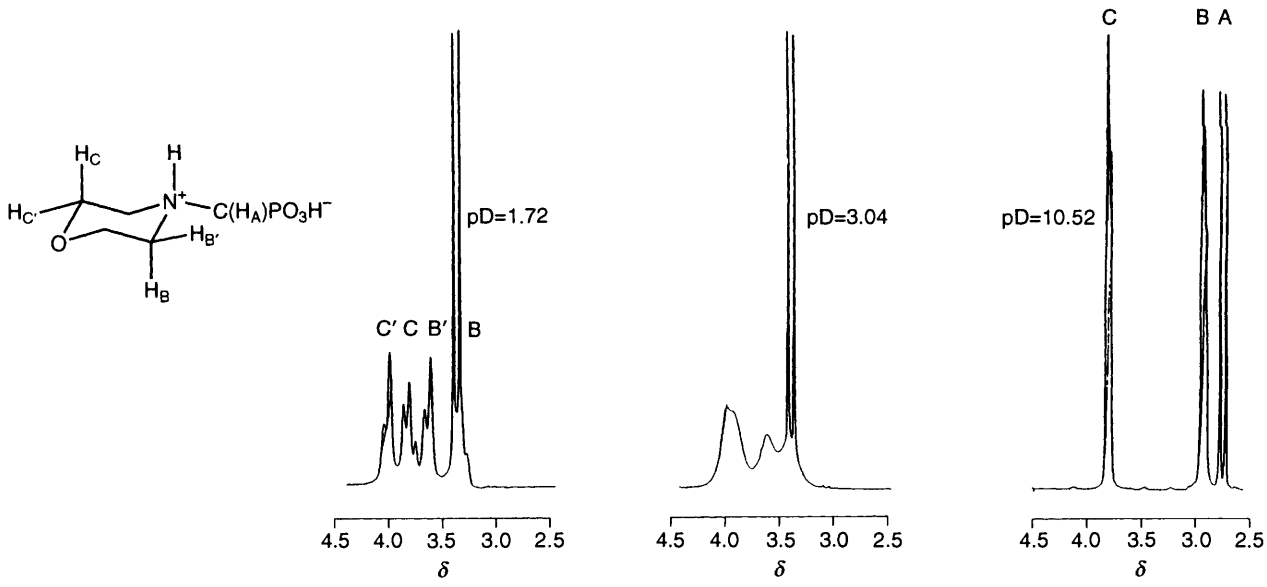

Fig. 1 ^{1}H NMR spectra for the pD titration of molecule **1**

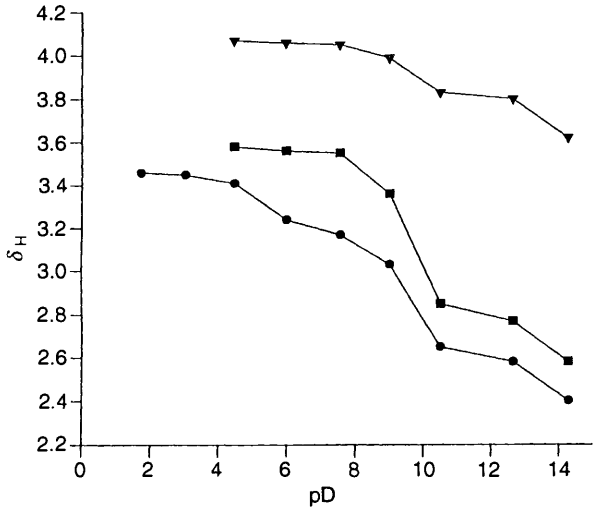

Fig. 2 Plot of pD *vs.* δ_H for molecule **1**: ●, A; ■, B/B'; ▼, C/C'

rapid and so the exchange processes fast. This is relevant especially for the ring protons.

The NMR spectra (^{1}H, ^{13}C and ^{31}P) of molecule **1** as it undergoes deuteriation give insight into the behaviour of both the morpholine ring and the appending $CH_2PO_3H^-$ group. Not only are the regions of deuteriation clearly defined, but also the dynamics of the molecule in solution are highlighted. Three distinct regions of behaviour are noted which are clearly visible in the ^{1}H NMR spectra. The regions correspond to different stages of motion in the molecule and correspond to the following ranges of pD: (*a*) pD = 14–6, (*b*) pD = 6–3, (*c*) pD = 3–0. In these regions the coupling pattern visible for morpholine ring protons changes in nature from an $(AA'BB')_2$ type at pD = 14–6, to an $(ABCD)_2$ type at pD = 3–0, consisting of separate signals for the individual axial and equatorial protons. 2D NMR techniques (COSY and HETCOR), ^{2}H NMR and NUMARIT computer simulations were employed in an attempt to verify the individual signals.

^{1}H *NMR*. The spectra are shown in Fig. 1 and a plot of pD *vs.* δ_H is shown in Fig. 2. The behaviour of the various signals in the ^{1}H NMR spectra as the titration progresses is fairly straightforward in terms of chemical shift and is similar to that observed by Lukeš[5] in the NMR study of piperidinylmethylphosphinic acid. At high values of pD when the molecule is fully undeuteriated the spectra consist of a sharp doublet corresponding to the H_A protons (caused by the $^2J_{PH}$ coupling) and a deceptively simple pair of 'triplet like' signals which correspond to the morpholine ring protons, actually, an $(AA'BB')_2$-type spectrum, the protons adjacent to the nitrogen $H_{B/B'}$ being shifted further upfield (1.0 ppm). As the pD of the solution is lowered all the signals undergo a downfield shift as the nitrogen becomes deuteriated in the range pD = 14–8. This is due to the deshielding process effected by the deuteriated nitrogen.[17] As the pD is lowered further from pD = 6–3 the ring protons experience little effect, however the methylenephosphonic protons (H_A) undergo a smaller downfield shift. This is due to the deuteriation of one of the phosphonate oxygens. The negatively charged oxygens exert a shielding effect which will be lowered as one of them becomes deuteriated resulting in a downfield shift.

The dynamics of the ring in solution add a complexity additional to that of the shift behaviour. As mentioned previously the ring protons give rise to an $(AA'BB')_2$-type coupling pattern at higher pD values. As a pD of 4.5 is reached the sharp triplet-type signals begin to lose their fine structure. The protons adjacent to the nitrogen $H_{B/B'}$ lose their fine structure first, then both sets proceed to form broad humps at pD = 3.04 and eventually form an entirely new, reasonably sharp, set of four signals at pD = 1.72, an $(ABCD)_2$-type spectrum. Such unusual behaviour is entirely due to the dynamic equilibria present in solution, which are dependent on the deuteriation state of the nitrogen. This is shown in Fig. 3 where at high values of pD, when the nitrogen is not deuteriated, rapid conformational change is possible *via* ring flipping and nitrogen inversion. These changes are fast, resulting in an averaging of the signals for the axial and the equatorial protons, the result of which is a deceptively simple three-line spectrum for each pair of protons in the $(AA'BB')_2$ coupling pattern. As the nitrogen begins to deuteriate several more equilibria are introduced into the system along with the aforementioned undeuteriated equilibria; an acid–base equilibrium will exist as well as the conformational change of the now deuteriated species. This gives rise to a multitude of signals and the subsequent broadening of the peaks observed at pD = 4.48. At very low pD values the ring becomes static as the nitrogen becomes fully deuteriated, *i.e.*, enters a region of slow exchange. Now nitrogen

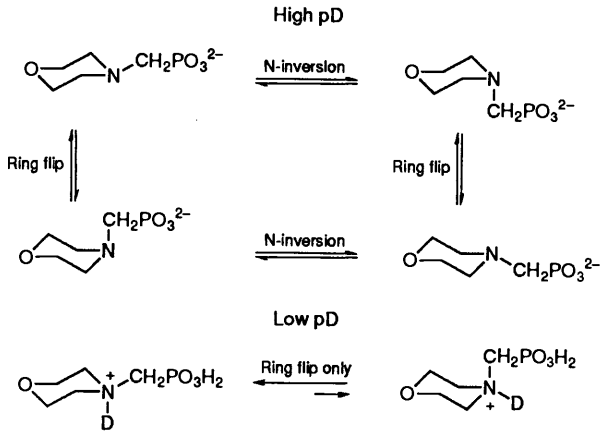

Fig. 3 Conformational change of molecule **1** at high and low pD

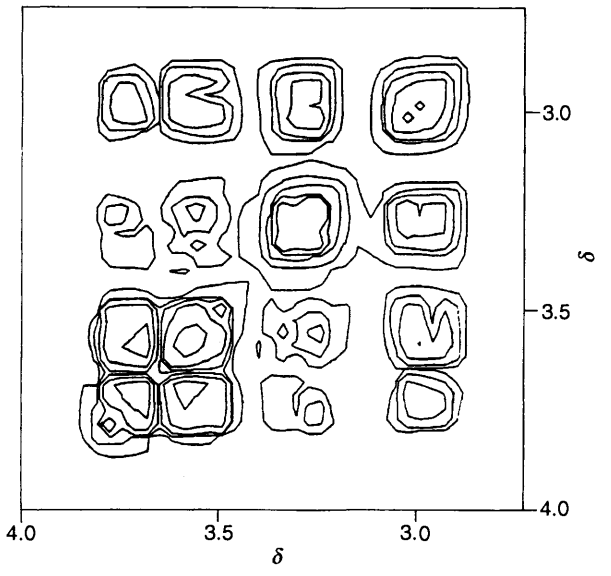

Fig. 4 2D COSY spectrum of molecule **1**

inversion is no longer possible due to the deuteriation, and only ring-flipping is possible.[8] To minimise unfavourable 1,3 diaxial interactions, the methylenephosphonic acid group favours an equatorial position as indicated by the solid state structure of the molecule (*vide infra*). Thus the equilibrium between the two states lies predominantly to the left. This results in a relatively static state, *i.e.*, the rate of exchange of conformers is sufficiently slow to allow the resolution of individual axial and equatorial protons [an $(ABCD)_2$-type coupling pattern].

Assignment of the individual signals to either axial or equatorial protons was attempted with the aid of 2D NMR, ^2H NMR spectroscopy and NUMARIT computer simulations. The evidence suggests the assignments are as follows, from low field to high field: $H_{C'}$, H_C, $H_{B'}$ and H_B. The protons next to the most electronegative atom, oxygen, would be expected to shift further downfield, as did their averaged signals at high pD. This was confirmed in a 2D HETCOR experiment. The two signals furthest downfield ($H_{C/C'}$) show a clear correlation with the ^{13}C signals for the C_C carbons, as do the furthest upfield signals ($H_{B/B'}$) with the carbon C_B.

A COSY 2D NMR experiment shows (Fig. 4) a very strong correlation between the two downfield protons H_C and $H_{C'}$ and also a strong correlation between the two upfield protons H_B and $H_{B'}$. The intensity of the contours is directly related to the magnitude of the coupling interaction and so it is clear that these are pairs of axial and equatorial protons and the interaction observed is the geminal coupling which is expected

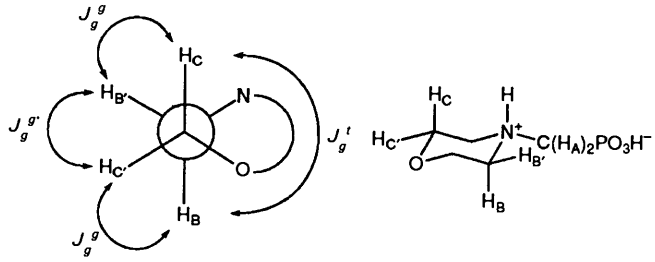

Fig. 5 Newman projection of molecule **1**

to be *ca.* −10 to −16 Hz. A Newman projection (looking down the morpholine C_C–C_B bond) is shown in Fig. 5 along with the various forms of coupling involved. The couplings between sets of protons consist of one $J_g^{g'}$, two J_g^g, and one J_g^t type coupling. Estimation of the magnitude of the couplings based on Pauling electronegativities using the method described by Abraham and Gatti[9] suggests the J_g^g values should be in the range 2–4 Hz with the $J_g^{g'}$ coupling being even smaller, but the J_g^t coupling interaction $\geqslant 12$ Hz. The Newman projection shows this larger interaction to be the one between the two axial protons H_B and H_C. Analysis of the COSY spectrum reveals the next largest interaction after the J_{gem} coupling interaction is that between the protons in positions 2 and 4 (in terms of upfield shift), *i.e.*, the ones from each pair which are furthest upfield. This is strong evidence for the assignment of these as axial protons. Equally compelling evidence is seen when considering the $J_g^{g'}$ and J_g^g couplings. The weakest interaction is calculated for $J_g^{g'}$ which corresponds to the coupling between the $H_{B'}$ and $H_{C'}$ protons. Analysis of the COSY spectrum, based on the assignments shows the weakest interaction to be that between these two protons. Slightly larger interactions of similar magnitude are observed for the J_g^g pairs of protons, *i.e.* $H_{C'/B}$ and $H_{B'/C}$ and again these were calculated as being slightly larger. The results from these two NMR experiments validate the assignments. The shape of the peaks shows the equatorial signals have a broad doublet-type shape whereas the axial protons exhibit a broad triplet-like shape: this is typically seen at low resolution. Further evidence can be gleaned from the NUMARIT simulation of the spectrum. Using the assignment of the signals from the 2D NMR experiments, a fit of the spectrum can be obtained. As further proof of the assignment, altering the coupling J_g^t constant affects the shape of the two signals shown as H_B and H_C only, *i.e.*, the two axial protons.

In a further attempt to confirm these assignments a natural abundance ^2H NMR experiment was performed on the sample. There is only a small isotope effect involved and ^2H chemical shifts generally correspond to their respective ^1H shifts. The relatively low natural abundance of ^2H of *ca.* 0.015% means coupling between deuteriums is minimised, *i.e.*, it is statistically unlikely that in any one molecule more than one deuterium will be present. Grant and co-workers[10] showed that the deuterium NMR spectrum for methylcyclohexane is resolved into individual deuterium resonances for the axial and equatorial deuteriums. It was thought that this method could be employed in the analysis of the axial and equatorial deuterium resonances for molecule **1**. An attempt to obtain the spectrum of a 40% w/v solution of molecule **1** in H_2O was made. However, only two broad signals were observed. They appeared in identical chemical shift ranges to the proton resonances. The broad peak at 3.7 ppm was thought to correspond to the deuteriums attached to carbon C_C and the peak at 3.1 ppm to the deuteriums attached to C_B and C_A. The lack of resolution proved disappointing. This may have been due to the field strength at which they were carried out (46.07 MHz) as the experiments performed by Grant were carried out at 76.77 MHz, but in addition, the solution used here was strongly acidic.

^{13}C *NMR*. A plot of pD *vs.* δ_C is shown in Fig. 6. The ^{13}C NMR spectra for molecule **1** simply consist of three sets of peaks: a singlet shifted downfield of all the rest corresponding to the carbons adjacent to the morpholine oxygen C_C, and two doublets further upfield, the smaller of which belongs to the other ring carbons C_B ($^3J_{PC}$ coupling) and the one of much larger coupling being the methylenephosphonic carbon C_A ($^1J_{PC}$ coupling). The methylenephosphonic carbon shows the expected behaviour on deuteriation, *i.e.*, as the nitrogen becomes deuteriated an upfield shift is noted as the carbon becomes increasingly shielded; this is followed by another upfield shift on deuteriation of one of the phosphonate oxygens which removes the deshielding effect of one of the P–O^- groups. These shifts occur in the same regions noted in the ^1H NMR spectrum for attached protons. The carbon C_C undergoes the first upfield shift as the nitrogen is deuteriated but is affected little by the second deuteriation of the phosphonate oxygen. The carbon next to the nitrogen, however, experiences no effect from either deuteriation, which is surprising as the related protons underwent large shifts. This behaviour can be attributed to the carbon lying outside any shielding area. The seemingly more distant carbons C_C were affected to a greater extent and must therefore lie inside this shielding area.

^{31}P *NMR*. The plot of pD *vs.* δ_P (Fig. 7) shows the standard shape of curve for a monophosphonic acid. Two distinct shifts in the molecule signal are noted, one large upfield shift (+ 8.6 ppm)

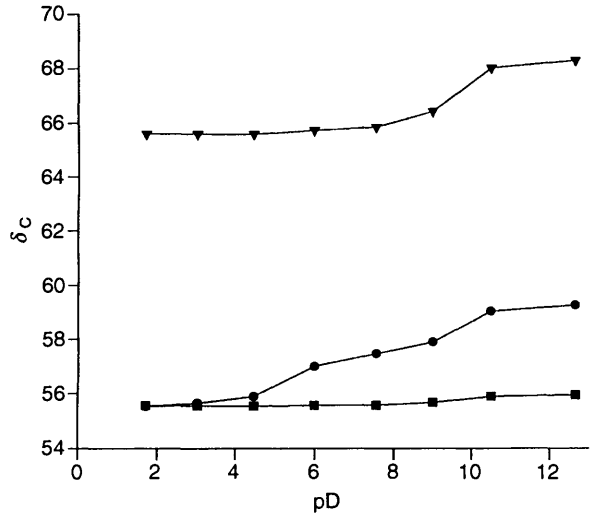

Fig. 6 Plot of pD *vs.* δ_C for molecule **1**: ●, A; ■, B; ▼, C

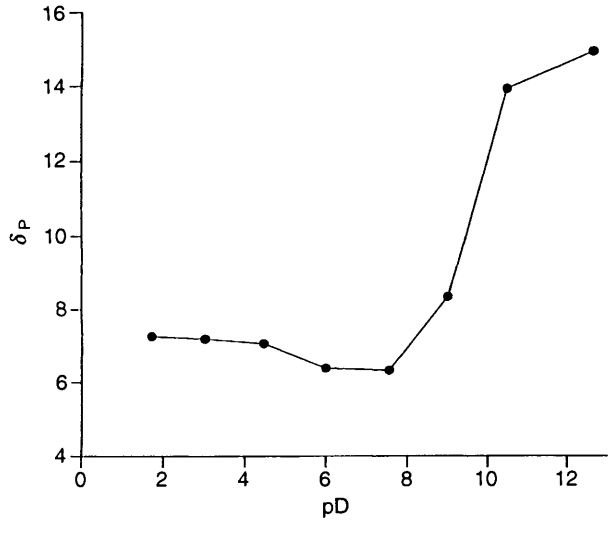

Fig. 7 Plot of pD *vs.* δ_P for molecule **1**

along with two smaller downfield shifts (– 1.0 ppm). The large upfield shift occurs in the range pD 14–10. This is due to the deuteriation of the nitrogen which causes a shielding effect on the phosphorus nucleus. Such an exceptionally large shift has been observed in the deuteriation of macrocyclic amines bearing methylenephosphonic acid groups and has been attributed to complexation of Na^+ within the macrocyclic cavity,[1] since titrations repeated with tetramethylammonium hydroxide instead of sodium hydroxide showed a reduced effect. However, a similarly large shift is present in the system being discussed and no macrocyclic cavity is present. These exaggerated shifts are clearly due to the complexation of Na^+, but may not necessarily have anything to do with a macrocyclic cavity. The formation of a five-membered chelate ring consisting of Na^+ and the phosphonate moiety at high pD is also a possible cause of this large shift.

A smaller downfield shift is observed in the range pD 6–4. This can be attributed to the deuteriation of one of the phosphonate oxygens causing a smaller deshielding effect. The deuteriation of the second phosphonate oxygen is shown by the second downfield shift at pD 2–1. The shape of the titration curve is of similar shape to that obtained in the titration of $NH_2CH_2PO_3H_2$ by Appleton *et al.*[7] which is to be expected for such a compound bearing only one phosphonic acid group. The ^{31}P signal forms a sharp triplet at all pD values, caused by the $^2J_{PH}$ coupling to the methylene protons H_A.

Coupling constants. Plots of the three coupling constants *vs.* pD are shown in Fig. 8. Each of the three coupling constants measured ($^2J_{PH}$, $^1J_{PC}$ and $^3J_{CNCP}$) shows the behaviour observed[11] in titrations of simple monophosphonic acids. The magnitude of each coupling constant decreases rapidly as the nitrogen becomes deuteriated and rapidly increases again as the phosphonate oxygen deuteriates giving rise to the typical U-shaped curve. The magnitude of the $^2J_{PH}$ coupling constant varies significantly responding to the deuteriation behaviour. As the first nitrogen is deuteriated the coupling constant becomes smaller (initially 12.2 Hz) reaching a minimum of 11.5 Hz at pD = 7.57. The coupling constant then begins to increase again as the pD becomes lower: presumably the deuteriation of the phosphate oxygen causes this. The $^2J_{PH}$ value continues to increase to a maximum value of 12.7 Hz at pD = 1.72.

The plots of $^1J_{CP}$ and $^3J_{CNCP}$ (Hz) *vs.* pD look almost identical with the plot of δ_P *vs.* pD; indeed they are almost superimposable given appropriate scales. This suggests these coupling constants are very sensitive to changes in their environment and not merely to the pD of the solution. In fact they give just as reliable information on the deuteriation behaviour of the species investigated as do the more conventional chemical shifts. Each plot shows a pronounced fall in magnitude of the coupling constant as the first nitrogen is deuteriated, followed by an increase again as the phosphonate oxygen becomes deuteriated.

Crystal Structure.—In the crystalline state as a monohydrate, morpholinomethylphosphonic acid has a zwitterionic structure which involves the deprotonation of one phosphonic acid group and the protonation of the nitrogen. The morpholine ring exists in a chair conformation with the methylenephosphonic group lying in an equatorial position. The structure is shown in Fig. 9.

The zwitterionic nature of the structure together with the presence of water of crystallisation results in extensive intermolecular hydrogen-bonding (Table 1 and Fig. 10) throughout the structure. In the *a* direction the molecules form chains of dimers. These are linked through the centre of symmetry by an asymmetric hydrogen bond of the type N–H···O with d(N···O) = 2.62 Å. The atoms involved in this dimeric structure [O(2), P, C(5), N, H(0), O′(2), P′, C′(5), N′ and H′(0)] form a ten-membered ring and are arranged in a

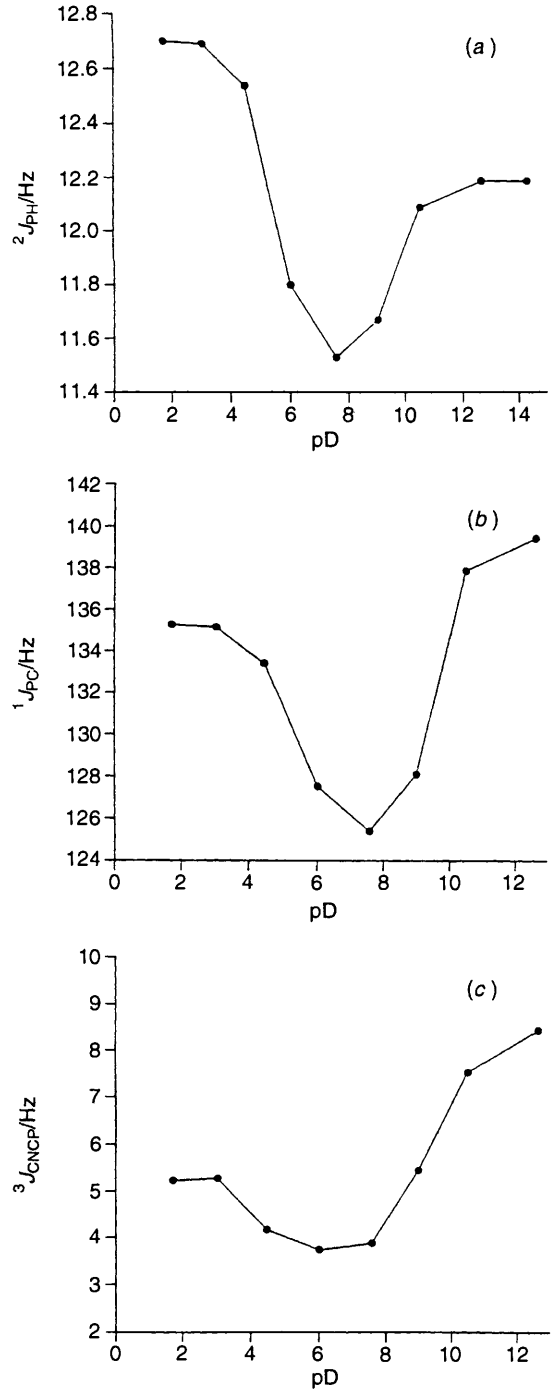

Fig. 8 Plots of coupling constants *vs.* $^2J_{PH}$ (*a*), $^1J_{PC}$ (*b*), $^3J_{CNCP}$ (*c*)

Table 1 Intermolecular hydrogen bonds for molecule **1**: distances (Å), angles (°)

Donor	Acceptor	Angle	O–H	O···O	H···O
O(5)–H(6A)	O(3)	165	0.87	2.78	1.93
O(5)–H(6)	O(1)	172	0.86	2.92	2.07
O(4)–H(4)	O(3A)	171	0.84	2.57	1.74
			N–H	N···O	H···O
N–H(0)	O(2A)	169	0.93	2.62	1.70

chair-like formation. This is similar to that observed for the dimeric structure of piperidinylaminomethylphosphinic acid[5] and aminomethyl(methyl)phosphinic acid.[12] In the *b* direction,

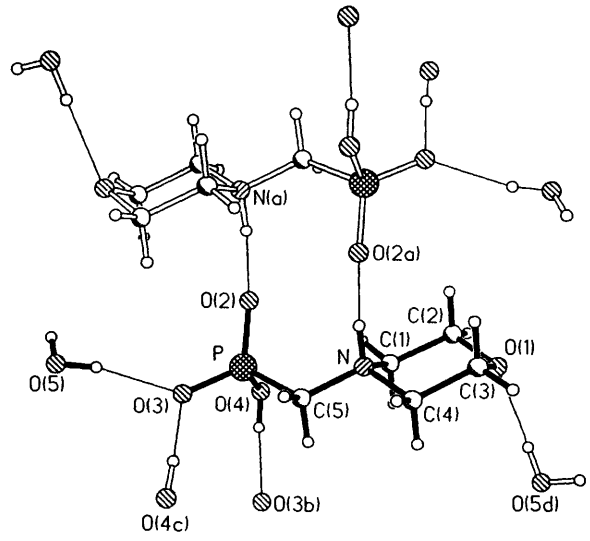

Fig. 9 Part of the crystal structure of **1**·H_2O. The asymmetric unit of the structure is shown with filled bonds and labelling of atoms. The centrosymmetrically related molecule completing the dimer unit is shown with hollow bonds. Hydrogen bonds (single lines) are shown to atoms in neighbouring molecules. Symmetry operations: *a*, $-x, 1-y, -z$; *b*, $\frac{1}{2}-x, -\frac{1}{2}+y, \frac{1}{2}-z$; *c*, $\frac{1}{2}-x, \frac{1}{2}+y, \frac{1}{2}-z$; *d*, $\frac{1}{2}+x, \frac{1}{2}-y, -\frac{1}{2}+z$.

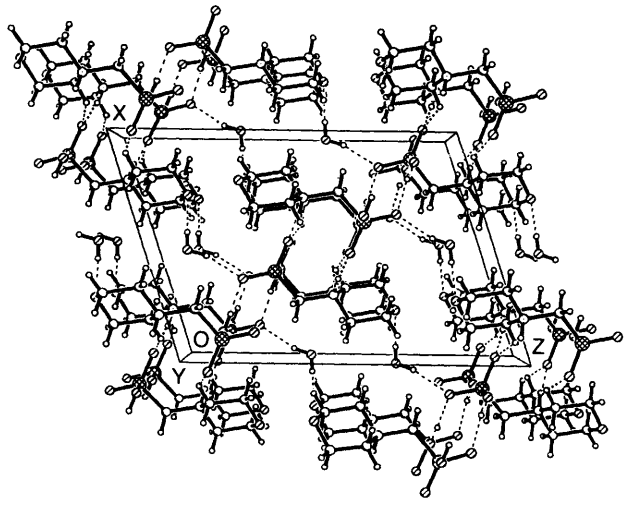

Fig. 10 Crystal packing, showing the hydrogen-bonding network (dashed lines). The view direction is almost the same as for Fig. 9.

the molecules are stacked with the morpholine rings parallel to each other, and are hydrogen-bonded to an adjacent parallel stack of molecules *via* P–OH(4)···O′(3)–P′ hydrogen bonds. In order to achieve these two types of interaction, all three oxygens attached to the phosphorus are involved in this complicated hydrogen-bonding network, *e.g.*, PO(2) is involved in holding the dimeric structure together, PO(3) and PO(4)H are hydrogen-bonded to two other dimeric pairs which also form the alternate stacks of parallel molecules. The water in the structure also plays an important hydrogen-bonding role, with both protons being involved. H(6A) is hydrogen-bonded to P–O(3) and the other proton, H(6) is hydrogen-bonded to the morpholine oxygen. The four different types of hydrogen bond in the structure are shown in Table 1 along with the angle, O–H···O, O···H, N–H···O and N···O distances.

In Table 2 are selected intramolecular geometrical data. The bond lengths agree well with the mean bond lengths for aminomethylphosphonic acid structures,[13] however the bond angles differ by up to 4° from the mean values, which may be a result of the extensive hydrogen-bonding. The angles in the

Table 2 Selected bond lengths (Å) and angles (°) for molecule **1**

P–O(2)	1.492(2)	P–O(3)	1.5051(14)
P–O(4)	1.572(2)	P–C(5)	1.830(2)
N–C(5)	1.495(2)		
O(2)–P–O(3)	118.18(8)	N–C(5)–P	116.22(12)

Table 3 Detailed breakdown of molecule **1**

m/z	Ion$^+$	Possible fragment lost	Possible structure
182	(M + 1)		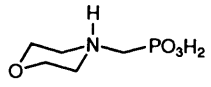
154	(M − 27)	CH_2CH_2	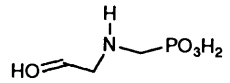
136	(M − 45)	CH_2CH_2OH	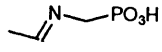
100	(M − 81)	PO_3H_2	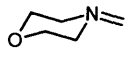
88	(M − 93)	CH_2PO_3H	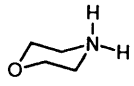
363	(2M + 1)		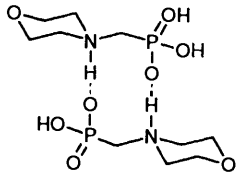
307	(2M − 55)	2 × CH_2CH_2	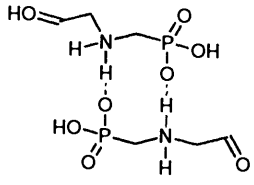

RPO_3 group deviate only slightly from those of a regular tetrahedron, except that the angle O(2)–P–O(3) is 118.18(8)°. This is an expected result of the repulsion of the two oxygens sharing the negative charge, and is also reflected in the P–O lengths. The P–OH length is 1.572(2) Å, *i.e.*, normal for a P–O single bond, whereas P–O(2) and P–O(3) are much shorter [1.492(2) and 1.5051(14) Å respectively] showing partial double-bond character.

FAB Mass Spectroscopy.—Aminomethylphosphonic acids are usually very impure: good methods of characterisation are thus important. While NMR spectroscopy has been used for characterisation in solution, and infrared spectroscopy and elemental analysis for solids, very little mass spectrometric work has been carried out. This has been due mainly to the very low volatility of this class of compound. In previous mass spectral studies, most involving multiple phosphonic acid groups, the acid groups are lost and neither molecular ion nor any significant breakdown pattern is observed. The monophosphonic acids on the other hand, gave interesting and useful

Table 4 FAB mass spectra for the principal ions of molecule **1**

Ion$^+$	*m/z*	%	Ion$^+$	*m/z*	%
(M + 1)	182	12.02	(2M + 1)	363	12.1
(M − 27)	154	100	(2M − 55)	307	13.3
(M − 45)	136	82.11	(2M − 73)	289	9.61
(M − 61)	120	13.35	(2M − 89)	273	4.27
(M − 81)	100	33.38	(2M − 105)	257	1.47
(M − 93)	88	34.20			
(3M + 1)	544	1.19	(4M + 1)	725	0.23
(3M − 83)	460	0.93	(4M − 111)	613	0.17
(3M − 100)	443	0.39			
(3M − 135)	408	0.33			

results in this work. Aggregates of the acid were observed at $(M + 1)^+$, $(2M + 1)^+$, $(3M + 1)^+$, and $(4M + 1)^+$. The abundances of these multiple ions diminished progressively as the aggregates increased in size. The structure of such aggregates could possibly be similar to that observed in the crystal structure of the molecule, where there is extensive intermolecular hydrogen-bonding throughout the structure. Based on a recent analysis of hydrogen-bonding in aminomethylphosphonic acids[4,13] and the crystal structure of molecule **1** specifically, potential structures for the aggregates using the same hydrogen bonding motifs are postulated (Table 3).

Characteristic breakdown patterns are observed for the molecule. A common feature in the breakdown of all the monophosphonic acid molecules investigated in this way[11] was the loss of the phosphonic acid group indicated by a peak at $(M - 81)^+$ ($M^+ - PO_3H_2$). A peak of high abundance was observed at *m/z* 93 which corresponds to the CH_2PO_3 fragment. The ions observed, along with their relative abundances are shown in Table 4. Most of the breakdown fragments from the oligomeric species must derive from the rings since the aminomethylphosphonic acid part is required to hold the monomers together; a suggested structure for the $(2M + 1)^+$ of molecule **1** is shown in Table 3 along with the possible residues relating to the breakdown of this molecule. An obvious pattern is the loss of fragments from $(M + 1)^+$ (loss of 28), $(2M + 1)^+$ (loss of 56), $(3M + 1)^+$ (loss of 84) and $(4M + 1)^+$ (loss of 112). This corresponds to 1 × 28, 2 × 28, 3 × 28 and 4 × 28 (where $CH_2CH_2 = 28$). The loss of successive CH_2CH_2OH is another pattern also noted for the oligomers M to 3M by the loss of multiples of 45 mass units.

Experimental

Instruments.—^1H and ^{13}C NMR were run on a Bruker WP200 spectrometer (^1H at 200.13 MHz, ^{13}C at 50.32 MHz). The ^{31}P NMR spectra were run on a JEOL FX90Q (36.2 MHz) spectrometer. The ^2H spectrum was obtained on a Bruker WB300 instrument. All ^{13}C spectra were broad-band decoupled. Elemental analysis was obtained on a Carlo Erba 1106 Elemental Analyser. The FAB mass spectrum was obtained from a methanolic solution using a KRATOS MS80RF. Operating conditions were accelerating voltage 4 kV, atom beam 8 kV with xenon bombarding atoms.

Preparation of Morpholinomethylphosphonic Acid (**1**).—This was prepared by a modification of the Moedritzer–Irani[14] synthesis of aminomethylphosphonic acids. Phosphorous acid (23.40 g, 0.28 mol) and morpholine (25.03 g, 0.29 mol) were dissolved in distilled water (50 ml). After slow addition of 37% w/v HCl (50 cm^3) the temperature was raised to reflux (*ca.* 110 °C) and 37% w/v aqueous formaldehyde (47.46 g, 0.58 mol) was added dropwise to the stirred solution over a period of 30 min. The reaction was then continued for a further 5 h after

which time the HCl–H_2O solvent mixture was concentrated almost to dryness and then taken up in 50% v/v ethanol (200 cm^3). The colourless crystalline product crystallised on addition of propan-2-ol (200 cm^3) and cooling. Yield (41.61 g, 75%), m.p. 255 °C (Found: C, 30.3; H, 7.1; N, 6.9. $C_5H_{12}NO_4P{\cdot}H_2O$ requires C, 30.2; H, 7.1; N, 7.0%); δ_H(200.13 MHz; D_2O; pD = 9.02) 3.03 (d, $^2J_{PH}$ 11.67 Hz, NCH_2P), 3.36 (m, OCH_2CH_2N) and 3.99 (m, OCH_2CH_2N); δ_C(50.32 MHz; D_2O; pD = 9.02) 57.90 (d, $^1J_{CP}$ 128.1 Hz, NCH_2P), 55.66 (d, $^3J_{CNCP}$ 5.47 Hz, OCH_2CH_2N) and 66.41 (s, OCH_2CH_2N); δ_P(36.2 MHz; D_2O; pD = 9.02) 8.35 (t, $^2J_{PH}$ 11.67 Hz).

NMR Titration of Molecule **1**.—A standard solution containing morpholinomethylphosphonic acid (0.26 mol dm^{-3}), sodium chloride (1.00 mol dm^{-3}) and *tert*-butyl alcohol (0.03 mol dm^{-3}) in D_2O was titrated with sodium deuteroxide (37% w/v). Samples were removed at regular pD intervals and their ^1H, ^{13}C and ^{31}P NMR spectra obtained. A high ionic strength was maintained by carrying out the titration in the presence of NaCl (1 mol dm^{-3}) (the amount of NaOD added being negligible compared with the original volume of solution). Bu^{t}OH was used as an internal reference. The chemical shift of Bu^{t}OH is known [15] to be largely independent of pD (δ_H = 1.3; δ_C = 31.6). The chemical shifts obtained in the titration were adjusted accordingly. The phosphorus chemical shifts were referenced to an external 85% H_3PO_4 solution. ^{13}C and ^{31}P NMR spectra for the pD titration of molecule **1**, along with the 2D HETCOR spectrum of **1**, are available as supplementary data.*

X-Ray Crystallography.—Crystal data for $C_5H_{12}NO_4P{\cdot}H_2O$. M = 199.14, monoclinic, space group $P2_1/n$, a = 10.679(4), b = 5.812(2), c = 14.938(6) Å, β = 107.80(3)°, U = 882.8(6) $Å^3$ (from 2θ values of 32 reflections measured at $\pm\omega$, $20 < 2\theta/deg < 25$), Z = 4, D_C = 1.498 g cm^{-3}, $F(000)$ = 424, μ(Mo-Kα) = 0.298 mm^{-1}, λ = 0.710 73 Å, T = 160 K.

Data collection and processing. All measurements were made on a Stoe-Siemens diffractometer equipped with a Cryostream cooler.[16] Intensities ($2\theta_{max}$ = 50°) were measured with ω/θ scans and on-line profile fitting.[17] Data reduction included corrections for Lp effects and standard reflection intensity variations; five standard reflections were remeasured after every 60 min of X-ray exposure time and varied by up to 1% in intensity. The variation of standard reflections was also used, together with normal counting statistics, to estimate standard deviations of intensities. No absorption corrections were applied. A total of 2046 measured reflections yielded 1556 unique data, with R_{int} = 0.0387.

Structure solution and refinement. The structure was determined by direct methods and refined by least-squares on F^2 values for all measured reflections.[18] Hydrogen atoms were included in geometrical positions using a riding model, except for those of the water molecule, for which the coordinates were freely refined. The hydroxy group was allowed to rotate as a rigid group about the P–O bond to find the best fit to the local electron density. Hydrogen atom isotropic displacement parameters were set to be 150% of those of the carrier atoms; all other atoms were refined anisotropically. The weighting scheme was of the form $w^{-1} = \sigma^2(F_o^2) + (0.0434P)^2 + 0.5700P$, where $P = (F_o^2 + 2F_c^2)/3$. Extinction effects were negligible. Final $wR = \{\Sigma[w(F_o^2 - F_c^2)^2]/\Sigma[w(F_o^2)^2]\}^{1/2} = 0.0892$ for all data, conventional R = 0.0305 based on F values of 1316 reflections having $F_o^2 > 2\sigma(F_o^2)$, goodness of fit = 1.061 on F^2 values, for 116 refined parameters. The largest residual peak in the electron density map was 0.36 e $Å^{-3}$ with all shifts in the final cycles being < 0.001 of the corresponding esd values. Tables of bond lengths and angles, atomic coordinates and displacement parameters are available from the Cambridge Crystallographic Data Centre. For details of the CCDC deposition scheme, see 'Instructions for Authors (1994)', *J. Chem. Soc., Perkin Trans. 2*, 1994, issue 1.

Acknowledgements

The authors are grateful for support from the EPSRC and Courtaulds Coatings plc for a CASE award (to M. P. L.) and for generous support for this work.

References

1 C. F. G. C. Geraldes, A. D. Sherry and W. P. Cacheris, *Inorg. Chem.*, 1989, **28**, 3336.
2 I. Lázár, D. C. Hrncir, W.-D. Kim, G. E. Kiefer and A. D. Sherry, *Inorg. Chem.*, 1992, **31**, 4422.
3 M. P. Lowe, J. C. Lockhart, W. Clegg and K. A. Fraser, *Angew. Chem., Int. Ed. Engl.*, 1994, **33**, 451.
4 W. Clegg, P. B. Iveson and J. C. Lockhart, *J. Chem. Soc., Dalton Trans.*, 1992, 3291.
5 I. Lukeš, K. Bazakas, P. Hermann and P. Vojtisek, *J. Chem. Soc., Dalton Trans.*, 1992, 939.
6 M. Kodoma and E. Kimura, *J. Chem. Soc., Dalton Trans.*, 1978, 1081.
7 T. G. Appleton, J. R. Hall, A. D. Harris, H. A. Kimlin and I. J. McMahon, *Aust. J. Chem.*, 1984, **37**, 1833.
8 A. Streitweiser and C. H. Heathcock, *Introduction to Organic Chemistry*, Macmillan, New York, 1985.
9 R. J. Abraham and G. Gatti, *J. Chem. Soc. B*, 1969, 961.
10 D. M. Grant, J. Curtis, W. R. Croasmun, D. K. Dalling, F. W. Wehrli and S. Wehrli, *J. Am. Chem. Soc.*, 1982, **104**, 4492.
11 M. P. Lowe, Ph.D. Thesis, University of Newcastle-upon-Tyne, 1993.
12 T. Glowiak and W. Sawka, *Acta Crystallogr., Sect. B*, 1977, **33**, 1522.
13 P. B. Iveson, Ph. D. Thesis, University of Newcastle upon Tyne, 1991.
14 K. Moedritzer and R. R. Irani, *J. Org. Chem.*, 1966, **31**, 1603.
15 Bruker Almanac, 1990.
16 J. Cosier and A. M. Glazier, *J. Appl. Crystallogr.*, 1986, **19**, 105.
17 W. Clegg, *Acta Crystallogr., Sect. A*, 1981, **37**, 22.
18 G. M. Sheldrick, SHELXTL/PC Users Manual, Siemens Analytical Instruments Inc., Madison, WI, USA 1990; SHELXL-93. *A Program for Crystal Structure Refinement*, University of Göttingen, 1993.

* Supp. Pub. No. 57021 (4 pp.). For details of the supplementary publications scheme, see 'Instructions for Authors (1994)', *J. Chem. Soc., Perkin Trans. 2*, 1994, issue 1.

Paper 4/02465F
Received 26*th April* 1994
Accepted 1*st June* 1994